Hydrodynamic Characteristics of the Pusher, Tractor and Schottel Types of the Azipod Propulsion System

Hossein Gholami [ID] [1]
Hassan Ghassemi [ID] [1]*
Guanghua He [2]
Reza Shamsi [3]

[1] Amirkabir University of Technology, Iran

[2] Harbin Institute of Technology, China

[3] Khorramshahr Univ. of Marine Science and Tech, Iran

* Corresponding author: *gasemi@aut.ac.ir (Hassan Ghassemi)*

ABSTRACT

The main purpose of this paper is to investigate the hydrodynamics performance of the three types (pusher, tractor and Schottel) of the azimuthing podded drive (AZIPOD) electric propulsion system. To evaluate the propulsive performance of the podded drive system, the Reynolds-Averaged Navier Stokes (RANS) solver is employed. KP-505 propeller as the research object, hydrodynamic open-water characteristics of this propeller was first calculated, and agreed well with test results. Then, numerical simulation of the thrust, torque and efficiency of the three types of the AZIPOD systems (Pusher, Tractor and Schottel) with KP-505 propeller at various yaw angles (from -30° to +30° with 15° increments) and different advance coefficients were compared. For the Schottel propulsion system, the effects of the number of propeller blades and the blade pitch-diameter ratio on performance are presented and discussed. Finally, the effect of sturt, support element and pod for pusher type on the pressure coefficient, thrust and torque of one blade and whole blades is investigated during one cycle.

Keywords: Azimuthing podded drive (AZIPOD), KP-505 propeller, Numerical simulation, Hydrodynamic characteristics

INTRODUCTION

In the ship technology, the azimuthing podded drive (AZIPOD) propulsion systems play a significant role in the maritime industry due to advantages such as optimal energy management and outstanding dynamic performance. Among these systems, azimuth thrusters, powered by electric motors, provide the capability for 360-degree rotation, significantly enhancing the manoeuvrability of ships and marine vehicles. This technology, first introduced in 1951 by Joseph Becker, was applied in various fields including the protection of offshore platforms and vessels' positions, and due to its efficiency and operational capabilities, it leads to maintenance cost savings [1–3].

With many advantages of the AZIPOD propulsion system like generating thrust at multi-directional, providing excellent maneuverability, working in open-water flow causes to reduce the cavitation, compact and integrity systems are demanded by the owner to employ this system to the ships. For these reasons, naval architects are encouraged to pay attention and focus this system to investigate the hydrodynamic performance. Given the existing analytical and laboratory limitations, numerical simulation is recognized as a crucial tool for a better understanding and optimization of these systems. The current research, utilizing Star-CCM+ software, aims to accurately evaluate and compare the hydrodynamic performance of various azimuth propulsion systems to assist in more effective design and cost reduction in the industry [4,5].

AZIPOD propulsion systems, due to optimal energy management and excellent dynamic performance, have gained increasing popularity in the maritime industries. The modern

azimuth thruster, equipped with a Z-drive gearbox, in the Schottel company in Germany [6], was marketed as a rudder propeller [7]. The propeller is installed within a frame resembling a rudder and connected to a vertical shaft, allowing the system to transfer force to the propeller through the shaft while simultaneously rotating the force plane [8]. In this system, an electric motor is placed inside a casing that drives a fixed or controllable pitch propellers (FPP or CPP). The entire unit installed at the rear part of the ship can rotate up to 360 degrees around its vertical axis, thereby generating thrust in any direction and providing excellent maneuverability (Fig. 1),[9,10]. This device offers combined propulsion and maneuvering capabilities. The choice of propulsion type is based on hydrodynamic performance criteria, speed, and other factors.

AZIPODs are also used for dynamic positioning systems in offshore platforms and maritime vessels. For example, in drilling ships, thrusters are employed to maintain the ship's position against environmental forces such as wind, waves, and currents, and to generate thrust while transferring from one port to another [11]. The main advantages of using AZIPOD include maneuverability, the elimination of the need for a rudder, optimal electrical efficiency, efficient use of available space on the ship, and reduced maintenance costs. Ships equipped with azimuth thrusters do not require tugs for berthing, although in specific conditions and challenging locations, the use of tugs may still be necessary [12,13].
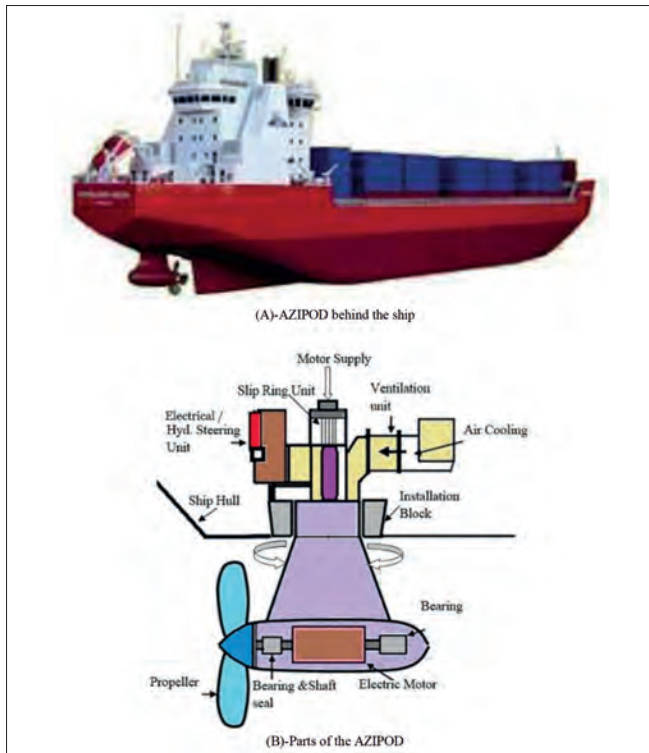

Fig. 1. AZIPOD propulsion system [14]

AZIPOD propulsion systems are utilized in various forms including tractor, pusher, and Schottel configurations. Given that an analytical solution to the equations governing the fluid flow around the propeller of these systems is practically unfeasible, and the costs of laboratory measurements are exceedingly high,

the importance of numerical simulation becomes increasingly evident. These simulations enable us to examine and compare the hydrodynamic performance of these types of propulsion systems using the commercial software of Star-CCM+ [15,16].

AZIPOD systems have been designed with and without duct. The pusher and tractor propulsion systems have a duct, which is intended to increase the efficiency of this type of propulsion system [17,18]. Ducted propellers may deliver higher efficiency in heavy and moderate conditions, while in light conditions may affect vice-versa. Generally, propellers for tug and fishing vessels use a ducted AZIPOD system to generate higher thrust by duct in heavy conditions.

METHODOLOGY

HYDRODYNAMIC CHARACTERISTICS

To evaluate the hydrodynamic characteristics of the ship propeller in the open-water condition is an important aspect to find the efficiency at different advance coefficients. The performance of the propeller depends on the geometries of the propeller like pitch-diameter ratio (P/D), number of blades (Z), expanded area ratio (EAR) and its blade section profile as well as operating condition (rotating speed and inflow velocity). If we consider the propeller rotates n under advance speed V (Fig. 2), the hydrodynamic open-water characteristics (K_T, K_Q, η) of the propeller is expressed as follows: [19].

$$K_T = \frac{T}{\rho n^2 D^4}, \quad K_Q = \frac{Q}{\rho n^2 D^5}, \quad \eta = \frac{J}{2\pi}\frac{K_T}{K_Q} \qquad (1)$$

where:
K_T – Thrust coefficient
K_Q – Torque coefficient
T – Thrust of propeller (N)
Q – Torque of propeller (N-m)
η – Propeller efficiency
J – Advanced coefficient ($J = \frac{V}{nD}$)
V – Advanced speed (m/s)
D – Diameter (m)
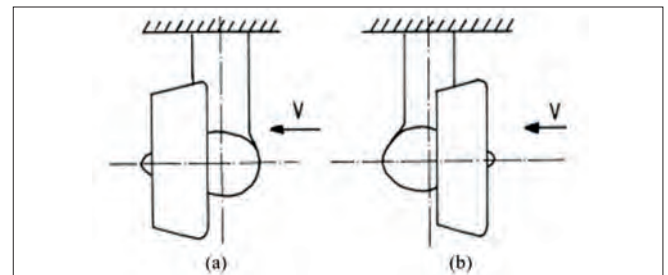n – Propeller rotation (RPS)
ρ – Water density (kg/m³)

Fig. 2. Azimuth propulsion systems: (a) Pusher (b) Tractor [20]

Additionally, the pressure coefficient (C_P) is an essential parameter to calculate the hydrodynamic performance. It is

defined by $C_P = \Delta P / \frac{1}{2}\rho V_R^2$, where V_R is the resultant velocity ($V_R = \sqrt{V^2 + (2\pi rn)^2}$) and $\Delta P = P - P_0$. The P and P_0 are the local pressure acted on the body and is the upstream reference pressure, respectively.

NUMERICAL METHOD

Star-CCM+ is a powerful computational fluid dynamics (CFD) software used for simulating and analyzing fluid flow, heat transfer, and related physical phenomena. It offers advanced tools for meshing, modeling, and post-processing, making it highly suitable for detailed simulations of complex systems. In this research, the method used is numerical, utilizing the Star-CCM+ software, which provides comprehensive capabilities for simulating fluid flow and analyzing hydrodynamic parameters. The primary goal of this project is to analyze and examine in detail the hydrodynamic parameters affecting the performance of the azimuth propulsion system in three different types: tractor, pusher, and Schottel. This study includes evaluating the impact of changes in the inflow velocity and different yaw angles on the efficiency of the propellers in the tractor and pusher propulsion systems, as well as examining the effect of the number of propeller blades and the ratio of blade pitch to blade diameter in the Schottel propulsion system.

MODELLING

Simulation of three types of propulsion systems has been conducted in Rhino software and the 3D model StarCCM+. Rhino, or Rhinoceros, is a versatile 3D computer graphics and computer-aided design (CAD) application. Known for its precision and flexibility, Rhino is widely used in various fields such as architecture, industrial design, and marine engineering for creating complex 3D models. Fig. 3 indicates three types of the AZIPOD system. The propeller is rotated by the electric motor located inside the pod. The pusher and tractor types have duct 19A and it is attached to the pod by two fins.
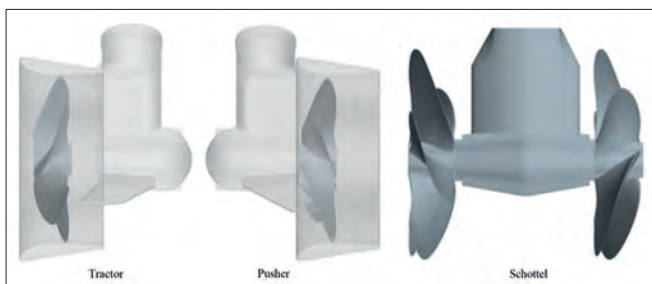

Fig. 3. Three types of AZIPOD

Conversely, in the pusher type azimuth propulsion system, the fluid flow initially passes over the thruster, meaning the thruster of this system is located upstream. The hydrodynamic geometry of both models is similar. Another distinction between these two types of azimuth systems can be noted in the orientation of their ducts. Since the objective of this project segment is to examine these two types of propulsion systems, the geometries of the models have been made as similar as

possible. However, the Schottel type propulsion system does not utilize a duct due to the presence of two propellers in this system. Nevertheless, the propeller geometry from both the pusher and tractor models has been employed.

GEOMETRY

For the simulation, geometries created using Rhino software are imported into the Star-CCM+ software under the 3D-CAD model section. To conduct the simulation, it is necessary to define several geometries such as the rotating region for the propeller, a refined region for better meshing, and a domain for performing CFD calculations. As illustrated in Fig. 4, we have utilized a semi-encapsulated domain because it allows us to have just one inlet and a pressure outlet, which significantly enhances the accuracy of our calculations.

MESHING

Mesh generation is a pivotal process in computational hydrodynamics, involving the subdivision of the computational domain and body surface into fine cells to accurately simulate fluid dynamics. This process employs a blend of surface, boundary layer, and volume meshes to adapt to complex geometries and focus computational resources on regions with high gradients of physical quantities like pressure and velocity. Particularly around areas of significant flow variation, such as propellers, denser meshing is essential for capturing the nuanced flow characteristics. The quality and accuracy of the mesh directly influence the convergence and reliability of numerical analyses.
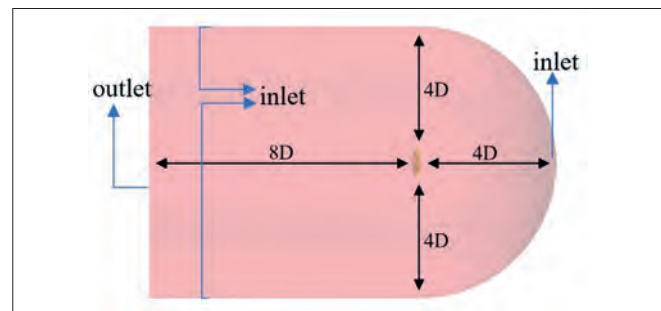

Fig. 4. Computational domain and boundary conditions
(D is the propeller diameter)

To avoid unnecessary computational costs and reduce computational time, mesh densification is applied in areas with high gradients of pressure, velocity, etc. As can be seen in Fig. 5, in the vicinity of the propeller where gradient changes are significant, a higher mesh concentration is required. To evaluate the quality of the model, a suitable mesh must be created and its accuracy examined. Techniques such as boundary layer meshing and controlled volumes are utilized to increase mesh concentration in areas with high gradients of pressure, velocity, and other critical variables. It is understood that after reaching a mesh independence threshold, the number of meshes will not significantly affect the output results; therefore, through multiple calculations using the STAR-CCM+ software, an appropriate

value for the number of meshes will be determined, which specifies the cell count used for each azimuth propulsion system type as listed in Table 1.

Tab. 1. Main dimensions of the KP-505 propeller

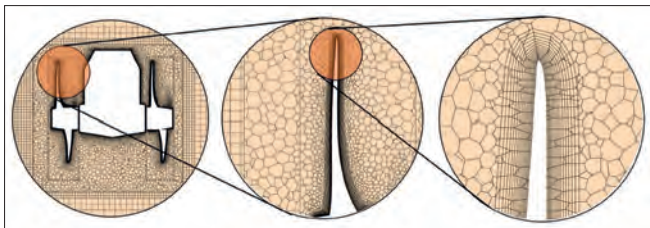| AZIPOD Type	Mesh for Propeller	Entire mesh
Tractor	1710K	2334K
Pusher	1034K	1760K
Schottel	3550K	4798K

Fig. 5. Schottel type propulsion system mesh

VALIDATION OF PROPELLER KP-505

In the project, the KP-505 propeller was utilized for the azimuth propulsion system. Fig. 6 shows the KP-505 propeller and more details of the main dimensions are given in Table 2 [21]. This propeller, due to its unique hydrodynamic characteristics, is a suitable choice for this type of propulsion system. The specific design of this propeller enables effective fluid flow guidance, thereby enhancing the overall system efficiency.
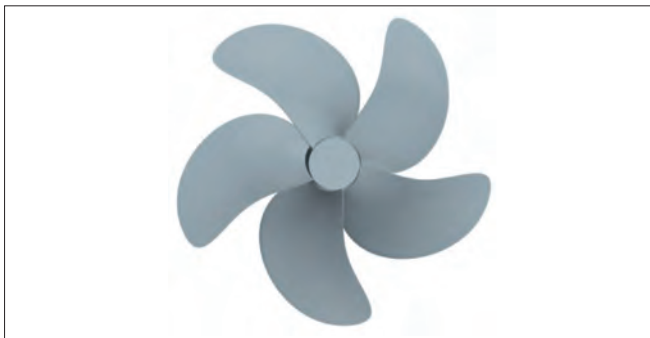
Fig. 6. Model propeller of KP-505

Tab. 2. Main dimensions of the KP-505 propeller

Parameters	Value
Diameter [m]	0.250
Hub diameter ratio	0.180
Pitch ratio (P/D)	0.950
Expanded area ratio (EAR)	0.800
Number of blades (Z)	5
Blade profile type	NACA66 + a = 0.8
Rotational speed (RPS)	9.5

Prior to executing the simulations, the model must undergo validation. This is a crucial step that ensures the results are reliable and accurate. During this process, the present simulation results are compared with experimental data or the results of other validated simulations to verify the model's accuracy. This validation process provides confidence that the simulation model is trustworthy and generates precise results.

In the field of ship hydrodynamics, this validation step is particularly important to ensure the reliability of the simulation outcomes. Without this validation, it would not be possible to have full confidence in the simulation results. The software run was conducted until convergence was achieved for four advance coefficients, ensuring that further iterations did not result in any changes in the torque and thrust coefficients. Fig. 7 compared the hydrodynamic characteristics of the KP-505 propeller. It is shown that the present results are in good agreement with the experimental data (given from [22]). As can be seen, the present result of the effciency at J = 0.7 has less than 5% error with the experimental data. Thrust and advance velocity at this J(= 0.7) are obtained about 65 N and 1.66 m/s (3.23 knots), respectively.
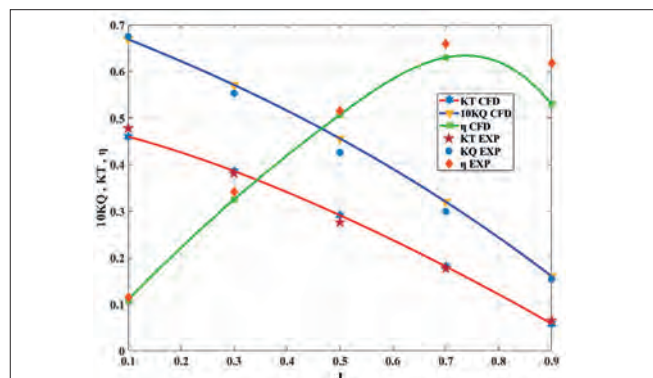

Fig. 7. Comparison of hydrodynamic characteristics of the KP-505 propeller

RESULTS AND DISCUSSIONS

In this section, we will present the results obtained from numerical simulations in the STAR-CCM+ software. In this simulation, effect of different values of the advance coefficient and yaw angle (Fig. 8) are investigated for all three types of AZIPOD. For the propulsion system of the Schottel (Fig. 9), some other parameters such as number of blades and pitch ratios are examined. Additionally, more investigations carried out for the pusher type during one cycle. Furthermore, the more numerical results under different yaw angles are presented and discussed.

Results of the pusher type

Simulations for the propulsion pusher system have been conducted at different advance coefficients and also at various yaw angles. Fig. 10 and Fig. 11 are shown the variations in thrust and torque coefficients versus advance coefficients under different yaw angles, respectively. As can be seen, with increasing the yaw angle on both directions (±30°), the thrust

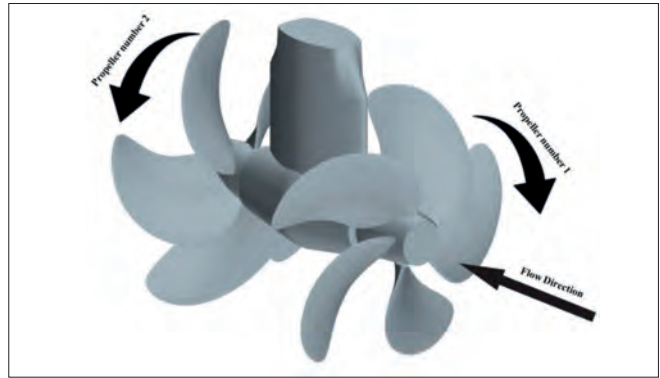*Fig. 8. Yaw angle about vertical axis*
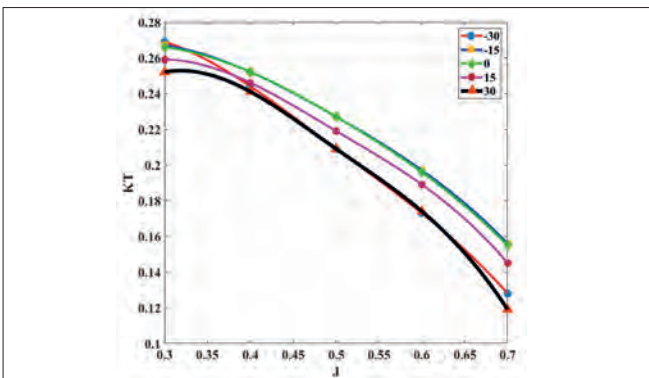

Fig. 9. Schottel type propulsion system

Fig. 10. Thrust coefficient versus advance coefficient under different yaw angles for the pusher type
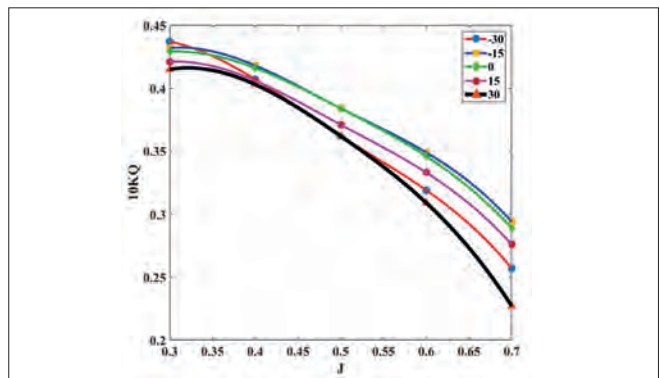

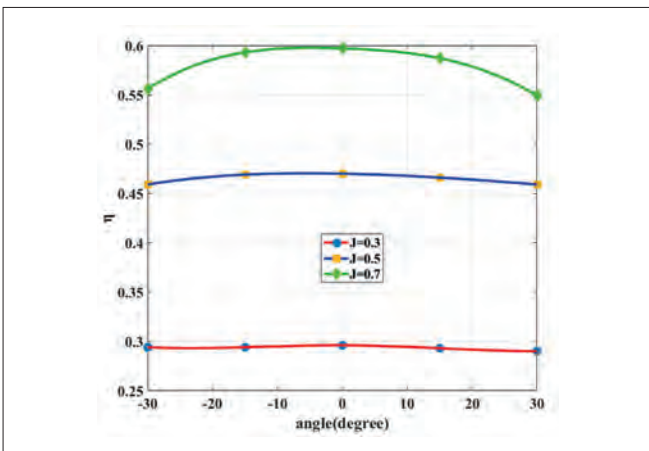*Fig. 11. Torque coefficient versus advance coefficient under different yaw angles for the pusher type*

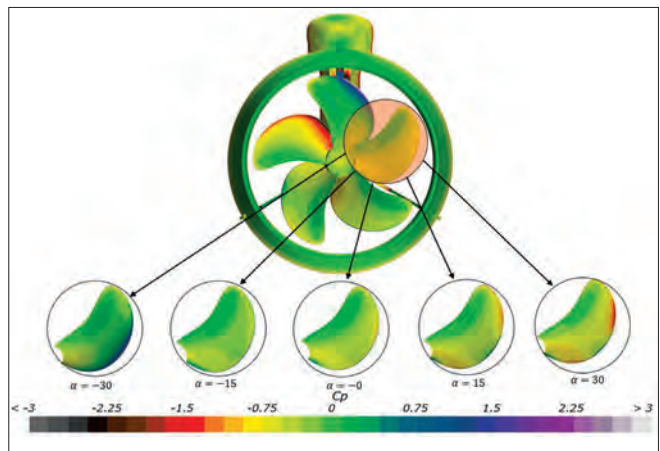*Fig. 12. Efficiency versus yaw angle under different advance coefficient for the pusher type*

Fig. 13. Pressure coefficient on a key blade of electric pusher type at J = 0.7 and various yaw angles

and torque coefficients are slightly decreased at low advance coefficient while significantly more decreases at high advance coefficient.

Fig. 12 demonstrates the effect of different yaw angles on the propeller blade. Upon examining this figure, it can be understood that varying yaw angles cause changes in pressure on the propeller blade. Specifically, an increase in the yaw angle results in increased pressure on the designated surface of the blade. Conversely, for the blade on the opposite side, the effect is reversed. Similarly, Fig. 13 illustrates the impact of the yaw angle on the pressure across all components of the propulsion

system at two different angles. This visualization allows for the observation of the pressure differential on the propeller's face between the left and right sides.

Fig. 14(a) and Fig. 14(b) display the streamlines on the propulsion system, allowing for the observation of how the propeller's advance coefficient influences the direction of flow. Additionally, If we compare Fig. 15(a) and Fig. 15(b), it is observed that in the strut part of this type of propulsion system, at a constant yaw angle, an increase in the coefficient of advance causes an increase in the pressure difference around the strut, which may also lead to flow separation.
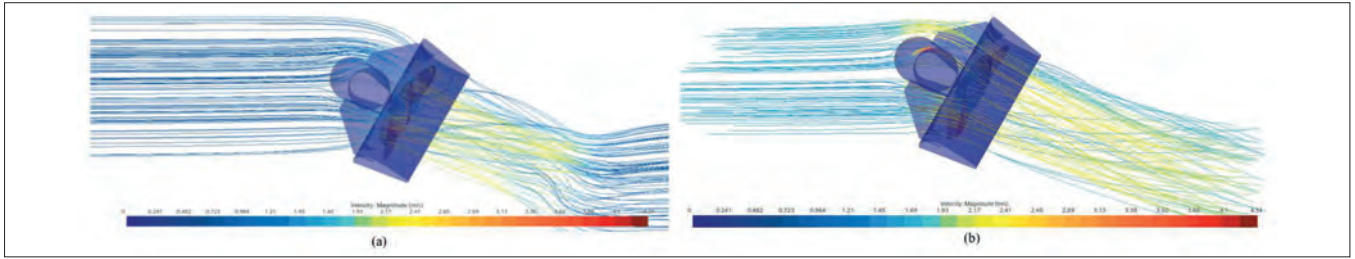
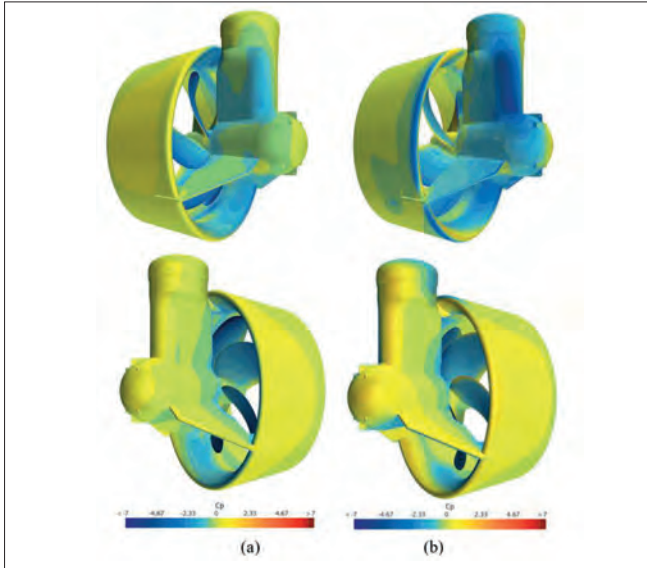Fig. 14. Streamlines around a pusher type, (a) J = 0.3, α = 30°, (b) J = 0.7, α = 30°

Fig. 15. Pressure coefficient around a pusher type,
(a) J = 0.3, α = 30°, (b) J = 0.7, α = 30°

Tab. 3. Hydrodynamic coefficients of the tractor type at two advance
coefficients (J = 0.3 and 0.7) and different yaw angles

J	Yaw angle (deg.)	T (N)	Q (N-m)	K_T	$10K_Q$	η
0.3	-30	111.8	4.415	0.309	0.489	0.302
0.3	-15	112	4.4	0.310	0.487	0.304
0.3	0	113.3	4.425	0.313	0.489	0.307
0.3	+15	113	4.435	0.313	0.491	0.304
0.3	+30	110.5	4.34	0.306	0.480	0.304
0.7	-30	54.9	2.66	0.152	0.294	0.575
0.7	-15	63.3	2.92	0.175	0.323	0.604
0.7	0	65.1	2.97	0.180	0.329	0.610
0.7	+15	62.6	2.89	0.173	0.320	0.603
0.7	+30	55.5	2.67	0.15	0.295	0.580
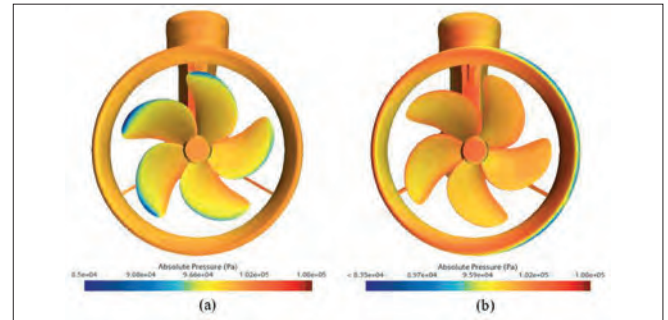
Fig. 16. Contour of pressure on a tractor type,
(a) J = 0.3, α =- 30°, (b) J = 0.7, α = -30°

Results of the electric tractor type

The AZIPOD electric propulsion system of the tractor type has a similar operational mechanism to the electric propulsion system of the pusher, but with the distinction that the propulsion system components are situated upstream. Another difference compared to the electric propulsion system of the pusher is that the propeller has a counterclockwise rotation.

Since the KP-505 propeller, which is the subject of our study, is a clockwise propeller in this simulation, it is necessary to edit this type of propeller and rotate its blades 180 degrees around its axis to convert it to a counterclockwise KP-505 propeller. The mesh settings, setup, and other configurations are similar to the simulation of the pusher type.

The hydrodynamic coefficients for the tractor type are presented at two advance coefficients (J = 0.3 and 0.7) and different yaw angles in Table 3. The presented results in this table are almost the same trend with the pusher type. It is indicated

that with changing yaw angle from 0 to ±30° the efficiency is slightly decreased at J = 07, while it is almost constant at J = 0.3.

Fig. 16 indicates the absolute pressure on the AZIPOD tractor type propulsion system, with the propellers back visible. The pressure on the tip of the propeller (a) is lower compared to propeller (b). Additionally, on the right side of duct (b), a significant reduction in pressure is observed, which is due to its placement in a flow with higher inlet fluid velocity. Furthermore, Fig. 17 illustrates the streamlines on this propulsion system.
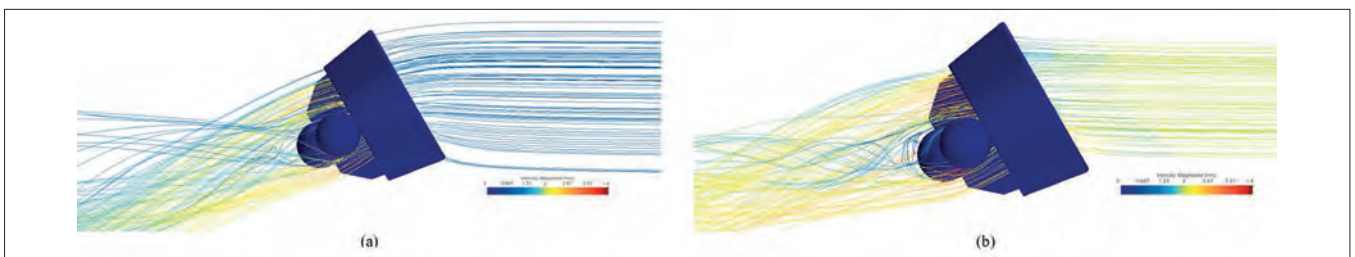

Fig. 17. Streamlines around a tractor type, (a) J = 0.3, α =- 30°, (b) J = 0.7, α =- 30°

Results of the electric Schottel type

The AZIPOD Schottel type system consists of two propellers: Fore propeller (Propeller 1), also known as the upstream propeller, and aft propeller (Propeller 2), the downstream propeller. This naming convention allows for the separate post-processing of each propeller's performance. Initially, the simulation of this azimuth propulsion system was conducted at various advance coefficients.

The pressure on the propeller number 1 and 2 of the azimuth propulsion system in Fig. 18 is observed. According to this image, the pressure of the propeller number 1 that is located upstream is greater than the pressure of the propeller number 2 that is located downstream. The hydrodynamic coefficient of this two propellers in Fig. 19 is clearly visible and it is evident that the propeller number 2 has a higher efficiency compared to the propeller number 1. At the advance coefficient of 0.7, the efficiency of Propeller number 1 is 0.625, while the efficiency of Propeller number 2 is 0.493. This advance coefficient exhibits the greatest efficiency difference between the two propellers. Fig. 20 shows the propeller wake at different cross-sections of upstream and downstream positions.
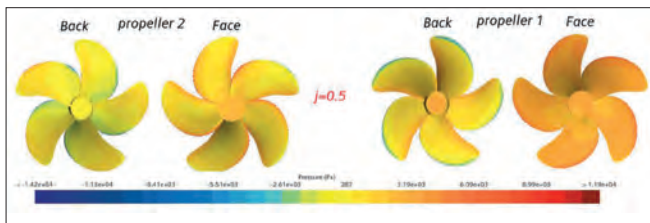

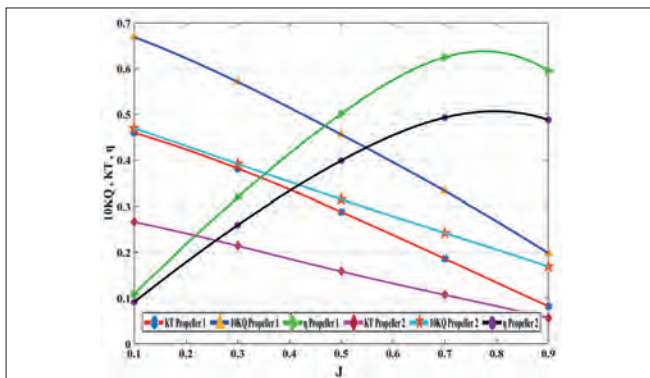*Fig. 18. Contour of the pressure on the propeller surface of a Schottel type at J = 0.5*

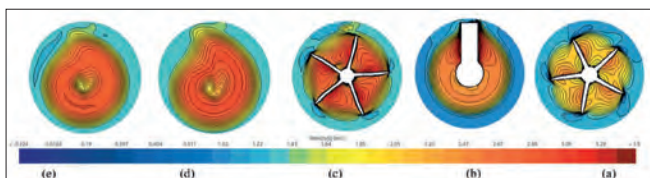*Fig. 19. Hydrodynamic open-water coefficient for Propeller 1 and Propeller 2 of the Schottel type*

Fig. 20. Propeller wake at different cross-sections position, J = 0.5, a) Section on propeller number one, b) Strut section, c) Section of propeller number two, d) Section at a distance downstream of propeller number two, e) Section at twice the propeller's radius downstream of propeller number two

Referring to Fig. 21, it can be observed how propeller number 2 neutralizes the rotational flow of propeller number one, and in the downstream of propeller number two, a uniform flow is created. This type of uniform, non-rotational flow is not present in other types of azimuth propulsion systems. In this section, the number of blades of propeller number two, which is a KP-505 propeller, has been increased and decreased. For each increase and decrease, separate software runs have been performed to determine the optimal number of blades for this type of propeller to achieve the highest efficiency. Table 4 presents thrust, torque and their coefficients under different blade numbers for Schottel type at J = 0.7, As shown in table, by increasing the blade number, the thrust and torque are increased but efficiency decreases.
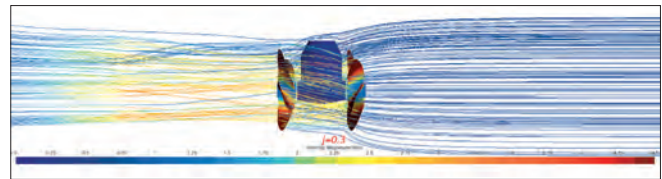

Fig. 21. Streamline around the Schottel type at J=0.3

Fig. 22 shows the two images on the right-hand side show the pressure coefficient on the blade number 4 with 6 (Z = 4 and 6). The two images on the left-hand side show the pressure coefficient on the blade of propeller number 2 with 4 blades. This information is essential for understanding the loading pattern and identifying potential regions prone to cavitation inception. It is noteworthy that propeller number one has been intentionally hidden from view to enhance the visual clarity and focus on the hydrodynamic characteristics of propeller number two, facilitating a more detailed analysis of its performance in the context of ship propulsion systems. In the subsequent section, a parametric study has been conducted to examine the influence of the P/D of the blades on propeller number two on the overall propulsive efficiency of the system. The P/D is a critical design parameter that determines the axial distance traveled by the propeller during one complete rotation, relative to its diameter. In this analysis, the P/D ratio has been systematically varied from 0.85 to 1.55 (Table 5, and Fig. 23), covering a wide range of pitch settings. For each incremental change in the P/D, comprehensive numerical simulations have been performed to obtain the corresponding hydrodynamic performance parameters. The results of this parametric study, including thrust, torque, and efficiency coefficients are presented and discussed.

Tab. 4. Thrust, torque and their coefficients under different blade numbers (Schottel type propeller 2), J = 0.7

Number of blades	T (N)	Q (N-m)	K_T	K_Q	η
3	36.5	1.78	0.101	0.0197	0.5711
4	39.3	2.055	0.108	0.0227	0.5326
5	38.5	2.19	0.106	0.0242	0.4896
6	38.1	2.34	0.105	0.0259	0.4534

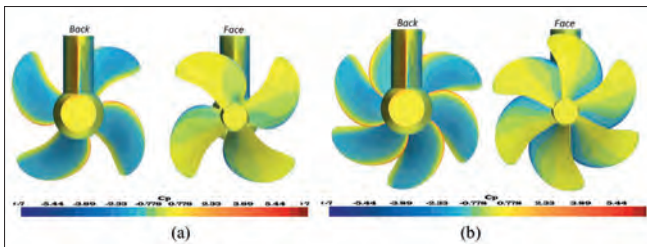| P/D	T (N)	Q (N-m)	K_T	K_Q	η
0.85	15.3	1.28	0.042	0.0141	0.3329
0.95	38.5	2.19	0.106	0.0242	0.4896
1.15	90.56	4.68	0.250	0.0518	0.5389
1.35	141.5	7.76	0.391	0.0858	0.5078
1.55	189.2	11.48	0.523	0.1270	0.4590

Fig. 22. Pressure coefficient contour on propeller number 2 with (a) Z = 4 and (b) Z = 6

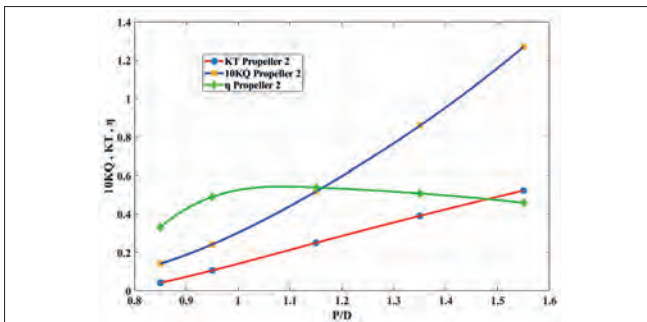

Fig. 23. Hydrodynamic coefficients versus P/D at J = 0.7

Finally, the hydrodynamic characteristics of the three types of the AZIPOD system against advance coefficients (from 0.3 to 0.9) are compared in Fig. 24. For the Schottel type, the fore and aft propellers (propeller 1 and propeller 2), the maximum efficiency is obtained about 0.64 and 0.52 at an advance coefficient of J = 0.775 and J = 0.8, respectively. For pusher type maximum efficiency is obtained 0.62 at J = 0.77, while for tractor type is around 0.63 at J = 0.82.
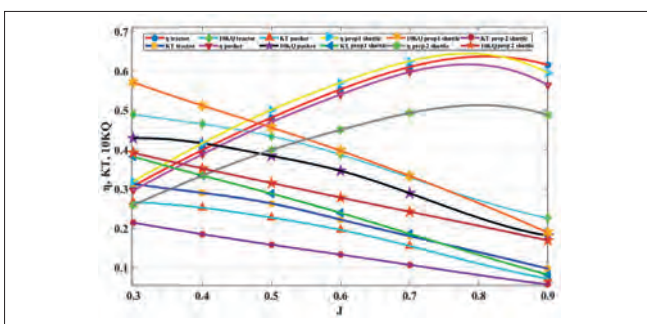

Fig. 24. Comparison of the hydrodynamic characteristics of three types AZIPOD systems

Results of pusher type in one cycle

In the puller type of the AZIPOD unit, the propeller receives a steady undisturbed wake field that is almost uniform and open water flow, while the propeller of the pusher type is located behind the pod, support elements and strut, the performance of the propeller is affected by these elements. For this reason, the impact of these elements on the propeller is investigated. As shown in Fig. 25, the rotation direction of the propeller in the pusher propulsion system is depicted from 0 to 360 degrees. To examine the influence of the pod, strut and support elements on the propeller performance, eight points (4 points at back and 4 points at face) are selected on a key blade, as illustrated in Fig. 26.
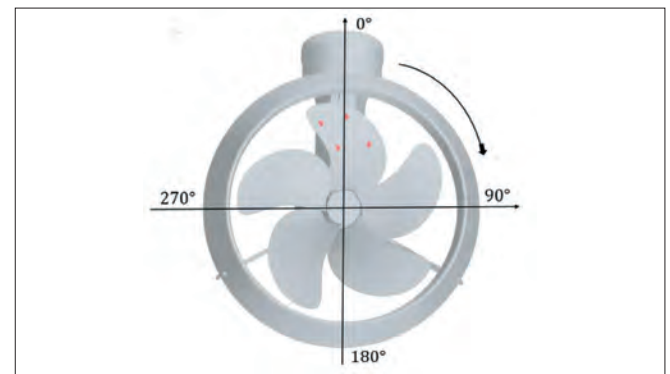

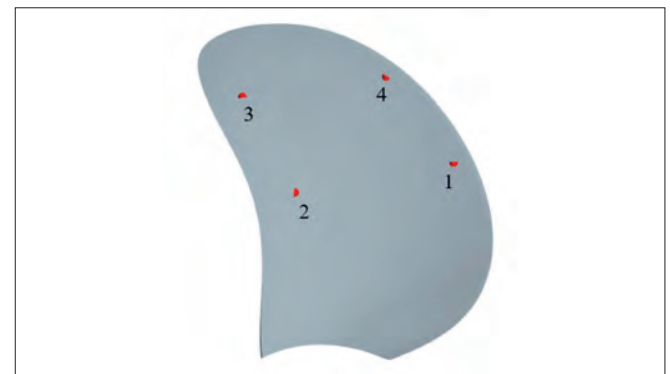Fig. 25. Direction of propeller rotation

Fig. 26. Four points at face side and four points at back side of the key blade (r/R=0.5, 0.8 and x/C=0.1 and 0.8)

Here, we present the results of pressure coefficient, thrust and torque coefficients at J = 0.3 during one cycle. Fig. 27 illustrates the pressure coefficient at 8 points on the blade. The pressure coefficient on the back side (suction side) and face side (pressure side) is negative and positive, respectively. Thrust and torque coefficients for one blade and whole blades during one cycle are shown in Fig. 28 and Fig. 29, respectively. For one blade, when the blade is positioned in front of the strut (θ or 360 *deg*), causes big amplitude and some fluctuations during one cycle due the support elements, as shown in Fig. 28. For whole blades, five small amplitudes can be seen during one cycle for both thrust and torque coefficients, as presented in Fig. 29. The average total thrust and torque coefficients (K_T and $10K_Q$) at J = 0.3 are found 0.27 and 0.43, respectively. For one blade is also obtained the average K_T and $10K_Q$ are found 0.056 and 0.085.
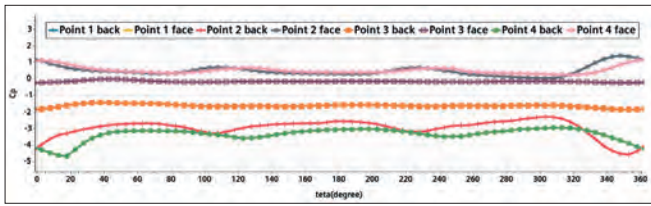
Fig. 27. Pressure coefficient of four points at back and four points
at face of the key blade (J = 0.3)
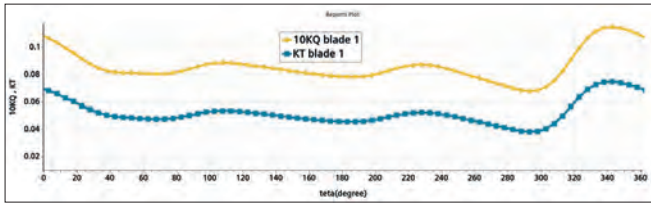

Fig. 28. Thrust and torque coefficients distribution of key blade
during one cycle (J = 0.3)

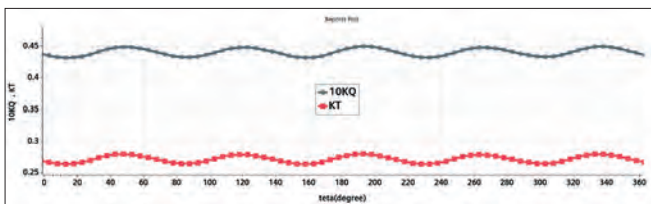

Fig. 29. Total thrust and torque coefficients distribution of propeller
during one cycle (J = 0.3)

CONCLUSIONS

This paper is numerically investigated the comparison of the hydrodynamic characteristics of the three types of the AZIPOD electric propulsion system (Pusher, Tractor and Schottel) under different operating coefficients. Based on the numerical results, the following conclusions can be drawn:

For the pusher and tractor:
- For both pusher and tractor types, with changing yaw angle from 0 to the efficiency is slightly decreased at J = 07, while it is almost constant at J = 0.3. The same trend is found for the tractor type.
- For pusher type, the efficiency at zero-yaw angle for J = 0.3 and J = 0.7 are obtained 0.296.and 0.597, respectively, while for tractor type, it is found 0.307 and 0.610, respectively.
- For pusher type, it is emphasised to show more details of the results of thrust and torque coefficients during one cycle. Some fluctuations for the pressure, thrust and torque are indicated due to strut, support element and pod.

For the Schottel:
- Propeller number 1 achieves its highest efficiency of 0.64 at an advance coefficient of 0.775, while propeller number 2 shows its maximum efficiency of 0.52 at an advance coefficient of 0.8.
- Effect of the blade number and pitch-diameter ratio on the performeance of the propeller number 2 are presented and discussed.

REFERENCES

1. Shamsi R, Ghassemi H, Molyneux D, Liu P. Numerical hydrodynamic evaluation of propeller (with hub taper) and podded drive in azimuthing conditions. Ocean Engineering 2014;76. https://doi.org/10.1016/j.oceaneng.2013.10.009.

2. Berchiche N, Krasilnikov V. I, Koushan K. Numerical analysis of azimuth propulsor performance in seaways: Influence of oblique inflow and free surface. J Mar Sci Eng 2018;6. https://doi.org/10.3390/jmse6020037.

3. Hu J, Zhao W, Chen C. G, Guo C. Numerical simulation on the hydrodynamic performance of an azimuthing pushing podded propulsor in reverse flow and rotation. Applied Ocean Research 2020;104. https://doi.org/10.1016/j.apor.2020.102338.

4. Shamsi R, Ghassemi H. Hydrodynamic analysis of puller and pusher of azimuthing podded drive at various yaw angles. Proceedings of the Institution of Mechanical Engineers Part M: Journal of Engineering for the Maritime Environment 2014;228. https://doi.org/10.1177/1475090213481417.

5. Fan X, Tang J. J, Zhang Y. X, Sun H. S, Gu Y. Q, Zhang J. X. Numerical investigation of the ship propeller load under reversed propulsion condition. Journal of Hydrodynamics 2021;33. https://doi.org/10.1007/s42241-021-0024-x.

6. SCHOTTEL. SCHOTTEL -schottel.de/en/home . (accessed online 10 Aug 2024).

7. Ghassemi H, Ghadimi P. Computational hydrodynamic analysis of the propeller-rudder and the AZIPOD systems. Ocean Engineering 2008;35. https://doi.org/10.1016/j.oceaneng.2007.07.008.

8. Huuva T, Törnros S. Computational fluid dynamics simulation of cavitating open propeller and azimuth thruster with nozzle in open water. Ocean Engineering 2016;120. https://doi.org/10.1016/j.oceaneng.2015.11.001.

9. Shamsi R, Ghassemi H. Numerical investigation of yaw angle effects on propulsive characteristics of podded propulsors. International Journal of Naval Architecture and Ocean Engineering 2013;5. https://doi.org/10.3744/JNAOE.2013.5.2.287.

10. Reichel M. Manoeuvring forces on azimuthing podded propulsor model. Polish Maritime Research 2007; 14:3–8. https://doi.org/10.2478/v10012-007-0006-0.

11. Liu P, Islam M, Veitch B. Unsteady hydromechanics of a steering podded propeller unit. Ocean Engineering 2009;36. https://doi.org/10.1016/j.oceaneng.2009.05.012.

12. Guo C. Y, Ma N, Yang C. J. Numerical Simulation of a Podded Propulsor in Viscous Flow. Journal of Hydrodynamics 2009;21. https://doi.org/10.1016/S1001-6058(08)60120-1.

13. Amini H, Sileo L, Steen S. Numerical calculations of propeller shaft loads on azimuth propulsors in oblique inflow. Journal of Marine Science and Technology (Japan) 2012;17. https://doi.org/10.1007/s00773-012-0176-z.

14. Majumder J. Control of Ship Electrical Motor Propulsion. Https://InstrumentationtoolsCom/Speed-Control-of-Ship-Electrical-Motor-Propulsion 2024.

15. Tu T. N. Numerical simulation of propeller open water characteristics using RANSE method. Alexandria Engineering Journal 2019;58. https://doi.org/10.1016/j.aej.2019.05.005.

16. Shamsi R, Ghassemi H. Time-accurate analysis of the viscous flow around puller podded drive using sliding mesh method. Journal of Fluids Engineering, Transactions of the ASME 2015;137. https://doi.org/10.1115/1.4027143.

17. Arief I. S, Musriyadi T. B, Je Mafera A. D. A. Analysis Effect of Duct Length– Nozzle Diameter Ratio and Tip Clearance Variation on the Performance of K-Series Propeller. International Journal of Marine Engineering Innovation and Research 2017;2. https://doi.org/10.12962/j25481479.v2i1.2527.

18. Arief I. S, Baidowi A, Ulfa M. Thrust and Torque Analysis on Propeller C4-40 with The Addition of Kort Nozzle to Pitch Variation. International Journal of Marine Engineering Innovation and Research 2021;6. https://doi.org/10.12962/j25481479.v6i3.10631.

19. Bernitsas MM, Ray D, Kinley P., KT, KQ and efficiency curves for the Wageningen B-series propellers. 237 1981.

20. Carlton J. S. Marine propellers and propulsion. 2018. https://doi.org/10.1016/C2014-0-01177-X.

21. National Maritime Research Institute (NMRI). https://www.t2015.nmri.go.jp/Instructions_KCS/instruction_KCS.html (accessed online 21 April 2024).

22. Lee S, Paik K. J. URANS simulation of a partially submerged propeller operating under the bollard condition. Brodogradnja 2018;69. https://doi.org/10.21278/brod69107.